International Journal on Advanced Science Engineering Information Technology

Vol.11 (2021) No. 2
ISSN: 2088-5334

The Effect of ANFIS Controller on The Performance of Induction Motor Drives in Low-Speed Operation Based on IFOC

Era Purwanto*, Indra Ferdiansyah, Syechu Dwitya Nugraha, Ony Asrarul Qudsi

Electrical Engineering, Politeknik Elektronika Negeri Surabayay, Jl Raya ITS Kampus PENS Sukolilo, Surabaya, 60111, Indonesia
**Corresponding author: era @pens.ac.id*

***Abstract*— The performance of the low-speed operation of induction motor (IM) drives has been discovered to be degrading and the performance of indirect field-oriented control (IFOC)-based IM drives depends on the efficiency of the inner loop Stator Current Regulator (SCR). Therefore, this research proposed the use of the Adaptive Neuro-Fuzzy Inference System (ANFIS) SCR to enhance the performance and optimize the operations of IFOC-based IM drives. It also compared the controller with PI SCR to analyze and evaluate the differences in how they perform. The results showed PI and ANFIS produced the same dynamic speed response trend and the use of ANFIS was able to reduce integral absolute error (IAE) up to 0.481% and phase current consumption from 2.78A – 6.32A both in peak and RMS value. Furthermore, there was a 29.29% - 45.58% reduction in the phase current total harmonic distortion (THD). This means the application of ANFIS SCR on IFOC-based IM drives enhanced the performance in the current constraint for high-performance purposes and low-speed applications.**

***Keywords*— IFOC; low-speed operation; stator current regulator; ANFIS.**

Manuscript received 27 May 2020; revised 27 Jan. 2021; accepted 3 Feb. 2021. Date of publication 30 Apr. 2021.

I. INTRODUCTION

The development of IM drives has increased along with a large number of IM utilization in the electric motor is driven system (EMDS), leading to approximately 60% of total electricity in the industry. It is, however, important to state that 69% of the total energy available is supplied to the industrial sector [1]-[3]. One popular revolution in IM drives is a vector or field-oriented control (FOC), commonly used to apply variable speed drives and motion control because of its superiority with high dynamic performance. It involves the decoupling of two components: flux and torque, which makes separate control possible as observed with separately excited DC motor treatment [1], [4]. In FOC drives, the indirect type (IFOC) is often used compared to direct ones (DFOC) because it is simple and effective without the need for sensor placement in the air gap for the acquisition of fluxes through computational techniques [1], [5].

IM is operated at nominal torque and speed, but it is at low speed in some applications. However, this low-speed operation causes performance degradation due to noise and vibration and, consequently, low power factor and efficiency [6]. This is associated with the low frequencies it operates and observed to be affecting the value of the stator resistance and slip requirements to produce torque. Moreover, an inverter's nonlinear characteristics for a low voltage range also make it difficult [7].

Therefore, it is necessary to control the speed, torque, flux, and current to produce high dynamic performance and improve the steady-state performance of IFOC which consists of two inner loops SCR, d-axis, and q-axis. Moreover, the high static and dynamic performance of IM drives depend on the inner loop [8], [9] such that it is possible to use d-axis SCR as a control variable for rotor flux while q-axis SCR is used for torque. Controlling the stator current on the dq-axis also affects forming the phase current of the IM formed by the current, voltage, and flux vectors in the dq-axis coordinate system [10]. Besides the performance improvement of these drives, another issue often discussed is the optimization of their operations, and this is established on three objective functions: increased efficiency, increased power factor, and minimization of stator or phase currents [11]. Furthermore, in the discussion of phase currents performance, the parameter usually considered is the harmonics and the presence of this factor represents an increase in copper losses which constitutes the majority portion of losses usually recorded in IM [12].

Several studies have been conducted on the IFOC inner loop SCR issue to discuss the design of dq-axis SCR to produce high dynamic performance, efficiency optimization, and power loss minimization [13]. Generally, PI SCR is a standard used in the dq-axis SCR due to its ability to control signals in a wide range of frequencies, reliability, easy design, simplicity, and affordability [9, 14]. However, its major disadvantage is the difficulty of finding the best values of proportional and integral gains [13]. Moreover, several controllers include the model-based, requiring complex and detailed system modeling like sliding mode controller [15], [16]. Fuzzy Logic Controller (FLC) is also a popular topic in SCR because of its easy implementation, independent parameters, absence of detailed mathematical models, and the ability to handle nonlinear systems [5], [17], [18], [19], [20]. FLC's biggest challenge is determining the membership function (MF) with optimum distribution and the best simplest rule design [18]. Meanwhile, the Artificial Neural Network (ANN) offers other advantages such as learning mechanism, robustness, adaptation, and quickness, which can be used to generate rules and MF of FLC through ANFIS. Some ANFIS applications in FOC include estimators for speed [21], speed controller [22], [23], torque controller [24], and efficiency optimization [25]. Therefore, this article proposed the use of the ANFIS SCR for low-speed operation conditions of 10-20% rated speed to enhance performance through the optimization of IFOC-based IM drives operations. It was also focused on analyzing the dynamic speed performance, current consumption (in peak and RMS value), SCR error performance, and THD of phase current and also to compare ANFIS SCR with PI SCR for performance evaluation. However, the ANFIS SCR was only used on the d-axis SCR and applied to 10 HP IM drives with constant and varying loads validated through MATLAB/Simulink.

II. Materials and Method

This section describes the methodology of IFOC for induction motor drives and ANFIS stator current regulator. The first is an explanation about one of the methods of control for induction motor drive. Complex vectors form IM currents as represented in the dq-axis coordinate system. This also involves the combination of three-phase sinusoidal currents into stator current i_s rotating against a particular frequency as in Eq. (1) and as illustrated in Fig 1.

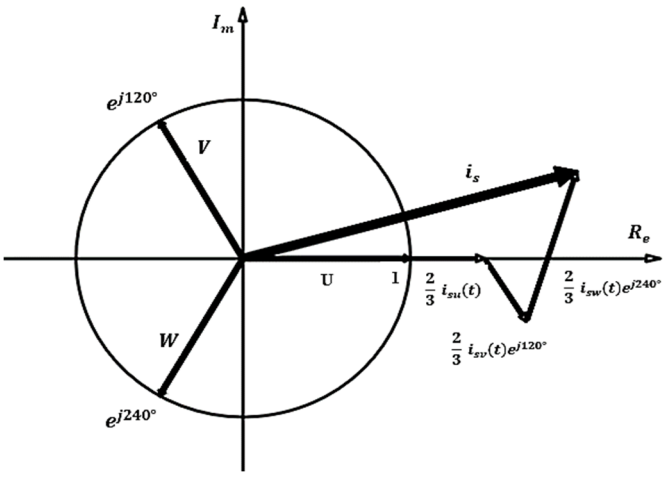

Fig. 1 Stator current formed by the phase current

$$i_s = \frac{2}{3}\left[i_{su}(t) + i_{sv}(t)e^{j\frac{2\pi}{3}} + i_{sw}(t)e^{j2(\frac{2\pi}{3})}\right] \quad (1)$$

Using this idea to combine other three-phase magnitudes such as complex vector voltages and flux linkages, it is possible to determine the angular speed as the circulate vector. Moreover, the dq-axis coordinate system rotating synchronously with all vectors divides three-phase magnitudes into two components, d and q. The equation of voltage, current, and flux linkage magnitude are expressed in Eq. (2)-(4).

$$u_s = u_{ds} + ju_{qs}; u_r = u_{dr} + ju_{qr} \quad (2)$$

$$i_s = i_{ds} + ji_{qs}; i_r = i_{dr} + jr_{qr} \quad (3)$$

$$\lambda_s = u_{ds} + j\lambda_{qs}; \lambda_r = \lambda_{dr} + j\lambda_{qr} \quad (4)$$

The division of two-component dq-axis coordinate systems, with the d-axis identical to the flux rotor and the q-axis to torque, leads to a condition where IM is linearized and treated like a separately excited DC motor. In FOC drives, IFOC is often used compared to DFOC and the block diagram of IFOC-based IM drives is shown in Fig. 2.

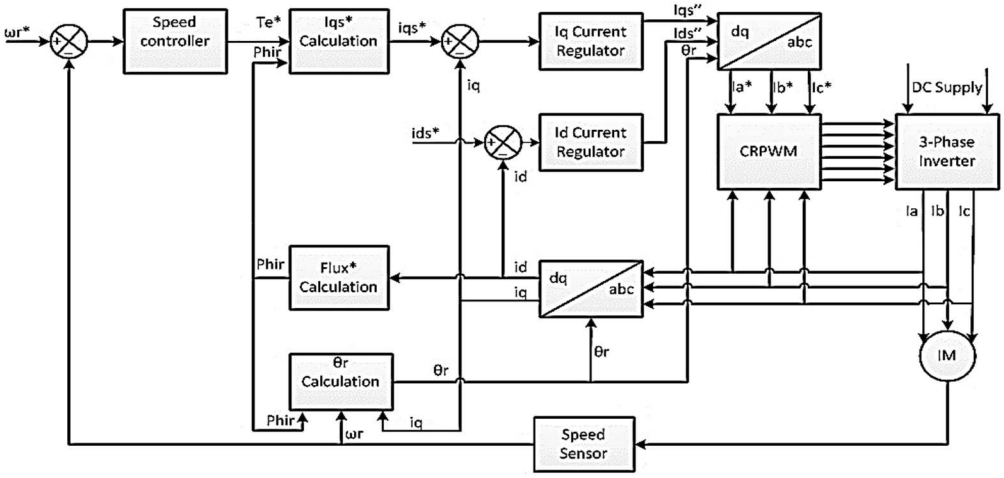

Fig. 2 Block diagram of IFOC-based IM drives

Four feedback signals are required in the process of IFOC. The first is rotor speed (ω_r) obtained from the speed sensor for the speed controller feedback to produce torque reference (T_e^*). This control signal serves as the input for the q-axis

stator current reference (i_{qs}^{*}) through Eq. (5) with additional flux estimation results ($Phir$) obtained by Eq. (6) and the slip speed calculated using Eq. (7). Meanwhile, the *d*-axis stator current reference value (i_{ds}^{*}) is needed.

$$i_{qs}^{*} = \frac{2}{3}.\frac{2}{P}.\frac{L_r}{L_m}.\frac{T_e^{*}}{|\lambda_r^{*}|} \quad (5)$$

$$|\lambda_r| = \frac{L_m.i_{ds}}{1+\tau_r s} \quad (6)$$

$$\omega_{sl} = \frac{L_m}{\lambda_r^{*}} * \frac{R_r}{L_r} * i_{qs}^{*} \quad (7)$$

Three other feedback signals are obtained from the stator current based on the current sensors converted to *dq*-axis stator current using Clark-Park transformation, which uses the coordinate transformation calculated in Eq. (8). Therefore, the equations of stationary reference frame conversion using Clark transform are expressed in Eq. (9)-(10).

$$\theta_e = \int(\omega_m + \omega_{sl})\,dt \quad (8)$$

$$i_\alpha = i_a \quad (9)$$

$$i_\beta = \frac{1}{\sqrt{3}} i_a + \frac{2}{\sqrt{3}} i_b \quad (10)$$

While the equations of rotating frame conversion using Park transform are expressed in Eq. (11)-(12).

$$i_{ds} = i_a.\cos(\theta) + i_\beta.\sin(\theta) \quad (11)$$

$$i_{qs} = -i_a.\sin(\theta) + i_\beta.cos(\theta) \quad (12)$$

The *dq*-axis stator current reference is subtracted by the *dq*-axis stator current from the transformation, produces an error, and is used as input for the two inner loops SCR. It has, however, being reported that the Performance of IFOC-based IM drives depends on its inner loop [8], [9]. The output of two inner loops SCR ($i_{ds}^{''}$ and $i_{qs}^{''}$) is input for inverse Clark-Park transformation as written in Eq. (13)-(14).

$$i_\alpha = i_{ds}''.\cos(\theta) - i_{qs}''.\sin(\theta) \quad (13)$$

$$i_\beta = -i_{ds}''.\sin(\theta) + i_{qs}''.\cos(\theta) \quad (14)$$

Therefore, the inverse of Clark transformation is shown in Eq. (15)-(17).

$$i_a = i_\alpha \quad (15)$$

$$i_b = -\frac{1}{2} i_\alpha + \frac{\sqrt{3}}{2} i_\beta \quad (16)$$

$$i_c = -\frac{1}{2} i_\alpha - \frac{\sqrt{3}}{2} i_\beta \quad (17)$$

The Clark-Park transformation output is used to produce the stator current reference required in the Current Regulator PWM (CRPWM) voltage source inverter (VSI), which are further used to feed IM drives by adjusting the frequency and magnitude of the three-phase signals.

The second is an explanation about FLC combined with artificial neural networks' learning ability is often known as ANFIS and usually starts with a structured framework. Meanwhile, the level of learning flexibility is used to generate input and output MF by testing the available dataset [26]. Moreover, it is possible to arrange the dataset to be used for the training by removing the not-so-important data in order to update the process and obtain input-output information from the target system. Furthermore, the training process obtains the best response from the system, making it possible to check the output due to its linguistic structure easily. ANFIS uses the Sugeno fuzzy system as a result of computational efficiency and the use of multipurpose procedures, as shown in Fig 3. It is also important to note that it is structured in five layers with different functions [24]. A rule was set with two fuzzies using the if-then rules are obtained as follows:

Rule 1: If *x* is$A_1$and*y* isB_1then$f_1 = p_1$x+ q_1y+ r_1

Rule2: If *x* is$A_2$and*y* isB_2then $f_2 = p_2$x+ q_2y+ r_2

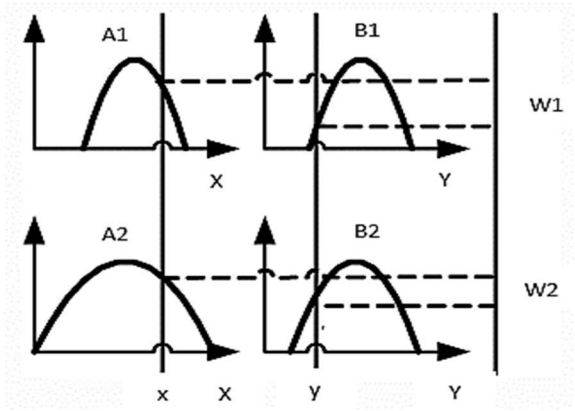

Fig. 3 Fuzzy Sugeno mechanism

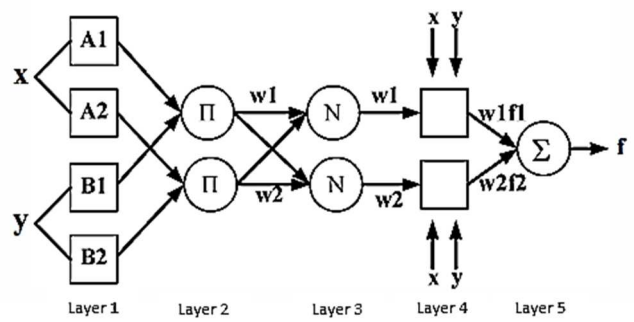

Fig. 4 The ANFIS structure with 2 input of fuzzy Sugeno

The architecture of ANFIS is shown in Fig. 4 with the node in each layer having the same function. For example, each node *i*n the layer *l* is$O_{l,i}$ and can be expressed with Eq. (18).

$$f = \frac{w_1 f_1 + w_2 f_2}{w_1 + w_2} = \overline{w_1} f_1 + \overline{w_2} f_2 \quad (18)$$

Layer 1: Each node in this layer is an adaptive node with output in Eq. (19)-(20).

$$O_{l,l} = \mu_{Ai}(x), \qquad for\ i = 1,2 \quad (19)$$

$$O_{l,i} = \mu_{Bi-2}(y), \qquad for\ i = 3,4 \quad (20)$$

Where x or y is the input node *i*, μ_A andμ_B are fuzzy set combined through the node function. The output of layer 1 is the MF value as the base part.

Layer 2: The node's function is to multiply the incoming signal, and each node in this layer is fixed with the output producing a degree of the fuzzy rule as shown in Eq. (21).

$$O_{2,i} = w_1 = \mu_{Ai}(x).\mu_{Bi}(y), \qquad i = 1,2 \quad (21)$$

Each output node represents the power of the rule.

Layer 3: Each node in this layer is fixed and the *i*-node adds up all the rules as represented in Eq. (22).

$$O_{3,i} = \overline{w_i} = \frac{w_i}{w_1 + w_2} \qquad i = 1,2 \quad (22)$$

Layer 4: Each node is an adaptive node and multiplied by the parameters *p, q,* and *r*as shown in Eq. (23).

$$O_{4,i} = \overline{w_i} f_i = \overline{w_i}(p_i x + q_i y \quad (23)$$

Where w_i is normalizing the degree of activation of layer 3 and $p_i q_i r_i$This node's setting parameter is used as a reference and can be obtained from the recursive least square estimator (RLSE).

Layer 5: A single node in this layer is fixed and processes all summations of inputs as depicted in Eq. (24).

$$O_{5,l} = \sum_l \overline{w}_i f_i = \frac{\sum w_i f_i}{\sum w_i} \quad (24)$$

Then, a distinct adaptive network like the Sugeno fuzzy model can be formed from layers 1 to 5.

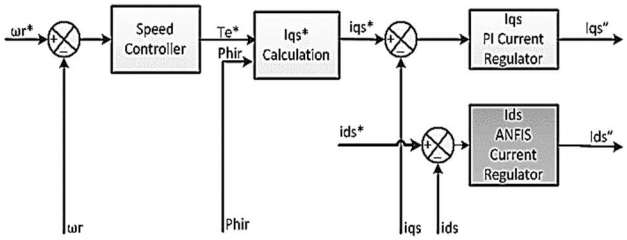

Fig. 5 IFOC-based IM drives with proposed ANFIS *d*-axis SCR

In this paper, ANFIS was applied to the *d*-axis SCR as shown in Fig. 5 and later used to analyze current performance. The structure of ANFIS used is shown in Fig. 6 with the composition of MF input 7x7 with a triangular type. Moreover, the hybrid training method was used in the ANFIS SCR with the output nodes moved to layer four by identifying subsequent parameters through the least square method in the forward pass of the training process. Error signals were sent back while parameters were updated by gradient descent in the backward pass. The parameter was identified optimally with a fixed premise condition. Therefore, the hybrid training method converged faster since it decreased the original backpropagation search space dimension [27].

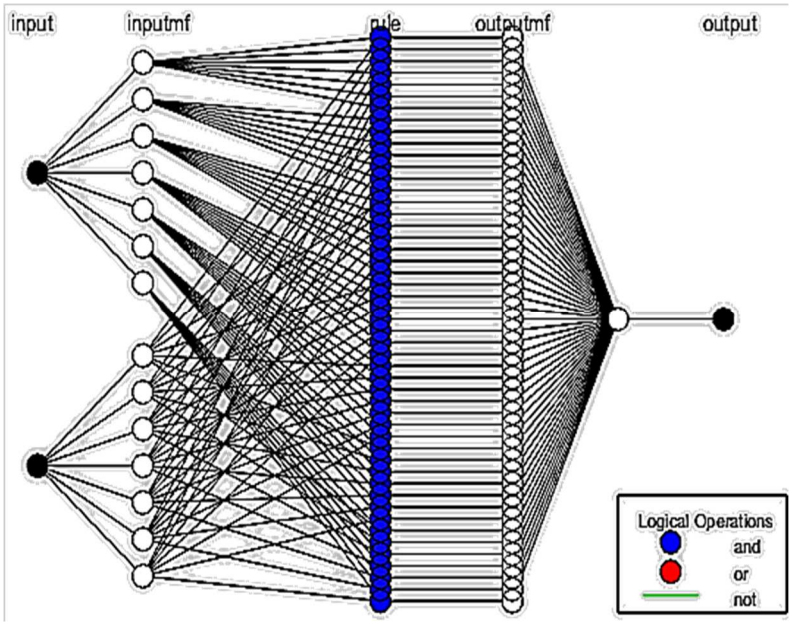

Fig. 6 Propose ANFIS SCR structure.

Inputs from the ANFIS SCR were error (e), delta error (Δe), and one output (Id''). The error was obtained from the *d*-axis stator current reference subtracted by the *d*-axis stator current resulting from the transformation, while the delta error was the current error subtracted by the previous error.

The plot error of the training results shown in Fig. 7 generated an error value of 0.157875%.

The ANFIS output was FIS as shown in Fig. 8, (a) is the MF for input error, (b) is the MF for input delta error, while the output had a linear value. Moreover, the surface viewer used to test the surface output of a FIS is presented in (c).

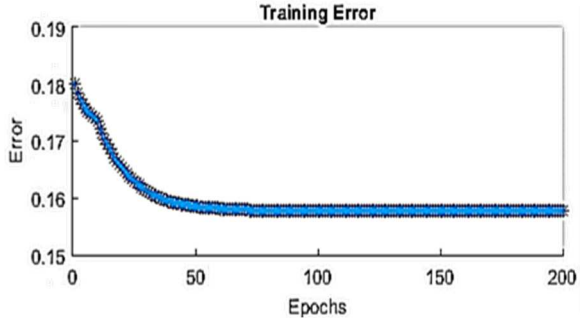

Fig. 7 The training error results.

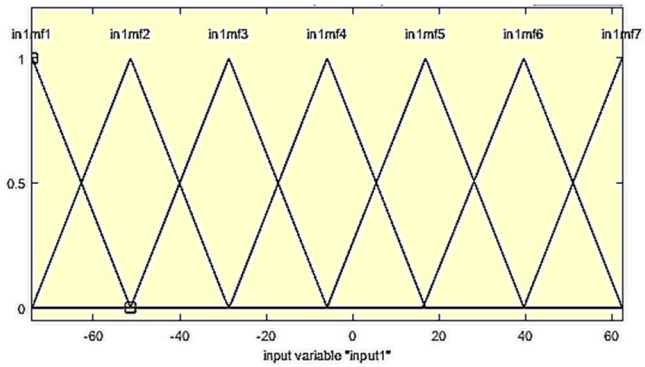

(a)

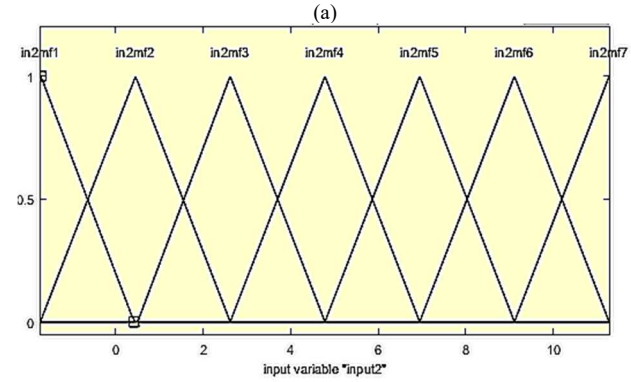

(b)

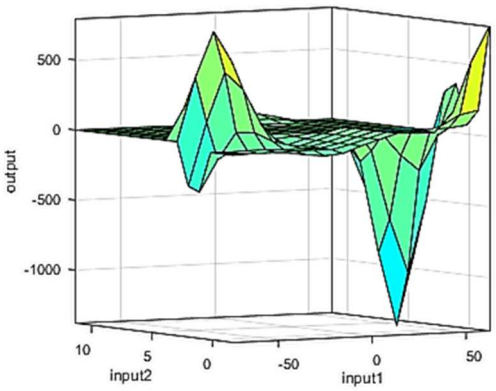

(c)

Fig. 8 (a) MF of input error, (b) MF of input delta error, (c) surface viewer

III. Result and Discussion

In order to evaluate the performance of ANFIS *d*-axis SCR, it was applied on 10 HP IFOC-based IM drives fed by CRPWM inverters via MATLAB/Simulink. Comparative evaluation studies were observed in two operating conditions, constant load and dynamic load, tested in the low-speed operation of 10-20% of 1500 rpm used as the rated speed. Moreover, the ANFIS *d*-axisSCR was compared with PI *d*-axisSCR regarding dynamic speed performance, phase current consumption, *d*-axisSCR error performance, and THD of phase current which was analyzed at a fundamental frequency of 50 Hz. The performance error of the *d*-axis SCR was obtained by using the IAE index expressed in Eq. (25) to represent the cumulative error, and this indicates the level of response concerning the reference [28].

$$IAE = \int_0^{\infty} |e(t)| dt \qquad (25)$$

A. Constant Load

For the constant load test, IM was operated in low-speed operation conditions with setpoints of 300 rpm which is the 20% of rated speed and 150 rpm which is 10% using 30 Nm and 10 Nm loads.

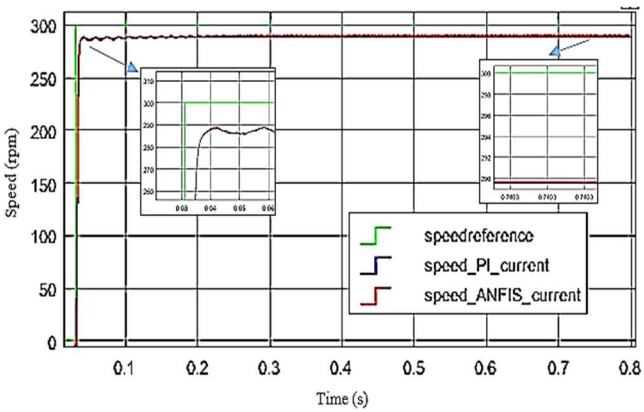

Fig. 9 Speed performance with set point of 300 rpm and 30 Nm load.

Figure 9 shows an IM operation's speed response performance at the 300rpm set point and a load of 30Nm. Through the use of PI, the IM accelerated to a steady-state speed of 0.106 s with 0.03486 s rise time, and the steady-state value achieved was 289 rpm with an error steady-state (ESS) of 3.6%. However, through the application of ANFIS, a settling time of 0.104 s with 0.03482 s rise time was produced at a steady-state value of 289 rpm and an ESS of 3.6%. This means the difference in the settling time for the two methods is 0.002 s, and the rise time value is 0.00004 s, while the steady-state values and ESS are equal.

The phase current and *d*-axis stator current performance are shown in Fig. 10 (a) and (b), respectively. It was discovered that at the phase current's peak value, the PI consumed 69.94 A while ANFIS consumed 63.62 A. For the RMS, PI consumed 35.89 A while ANFIS consumed 32.32 A in the phase current and 33.88 A on the *d*-axis stator current. Moreover, regarding the error performance of SCR, PI produced an IAE of 3.723% with a current ripple from -1.9 A to 4.5 A, while ANFIS produced 3.331% with a current ripple from -1 A to 4 A.

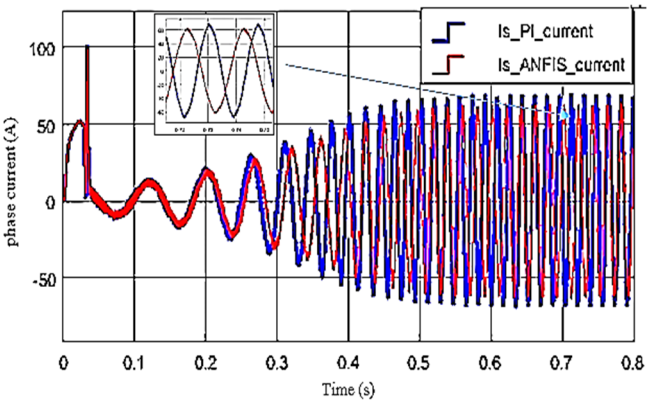

(a)

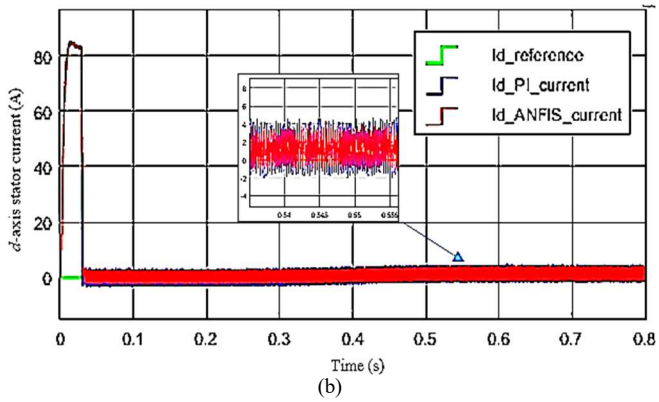

(b)

Fig. 10 Current performance with setpoint of 300 rpm 30 Nm.

Figure 11 shows the phase current THD's performance for the two methods, PI in (a) and ANFIS in (b). The results showed PI had a THD of 59.98% while ANFIS had 4.44%, indicating a difference of 55.54%.

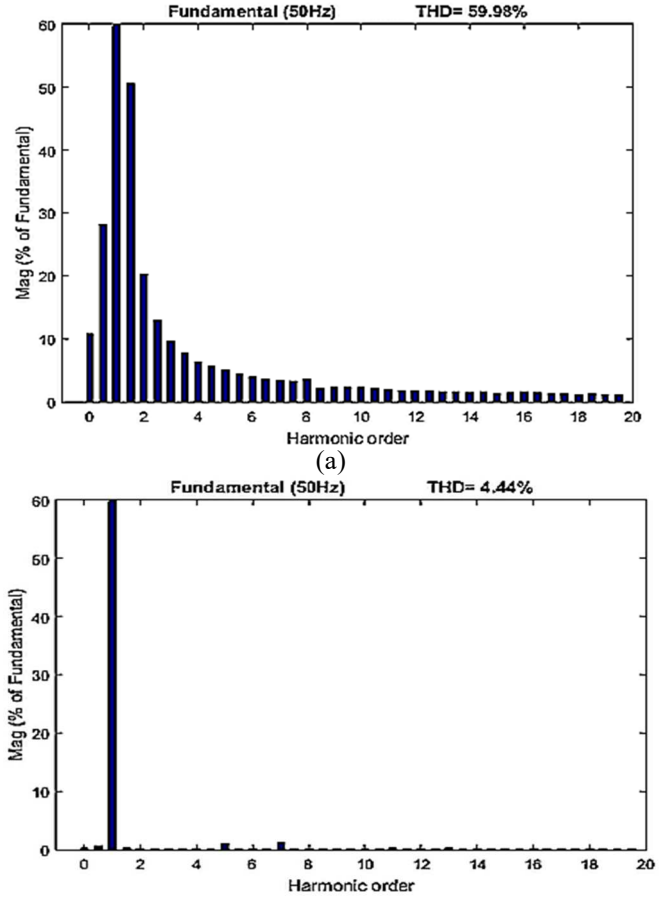

(a)

(b)

Fig. 11 THD of phase current with 300 rpm setpoint 30 Nm (a) PI *d*-axis SCR (b) ANFIS *d*-axis SCR.

At the same setpoint speed of 300 rpm, the load was changed to 10 Nm, and the dynamic speed response performance is shown in Fig. 12. Through the use of PI, the IM accelerated to a steady-state speed of 296rpm with ESS of 1.3% for 0.122 s with a rising time of 0.03472, while ANFIS also accelerated to 296 rpm with ESS of 1.3% but with a settling time of 0.090 s and a rising time of 0.03476 s. Therefore, the difference in the settling time is 0.032 s and the rising time value is 0.00004 s, while the steady-state value and ESS are the same.

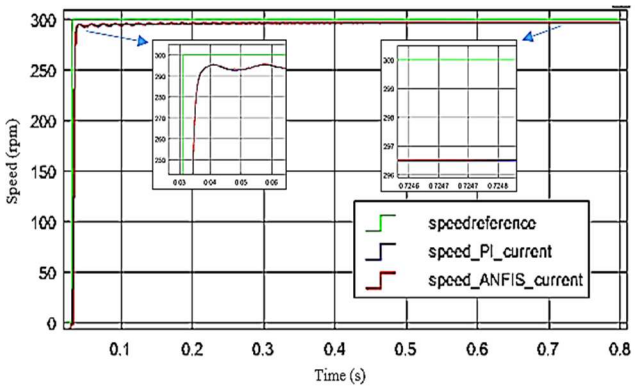

Fig. 12 Speed performance with set point of 300 rpm and 10 Nm load.

Figure 13 (a) and (b) are phase current and *d*-axis stator current performance, respectively. In a setpoint of 300 rpm with a load of 10 Nm, PI was found to have consumed 42.41 A in the phase current while ANFIS consumed 37.31 A, both in peak value. In RMS, PI consumed 20.29 while ANFIS consumed 17.51 A while in the error performance of SCR, PI produced IAE of 3.735% with current ripple from -2.2 A to 4 A while ANFIS produced 3.262% with current ripple from -1.8 A to 3 A.

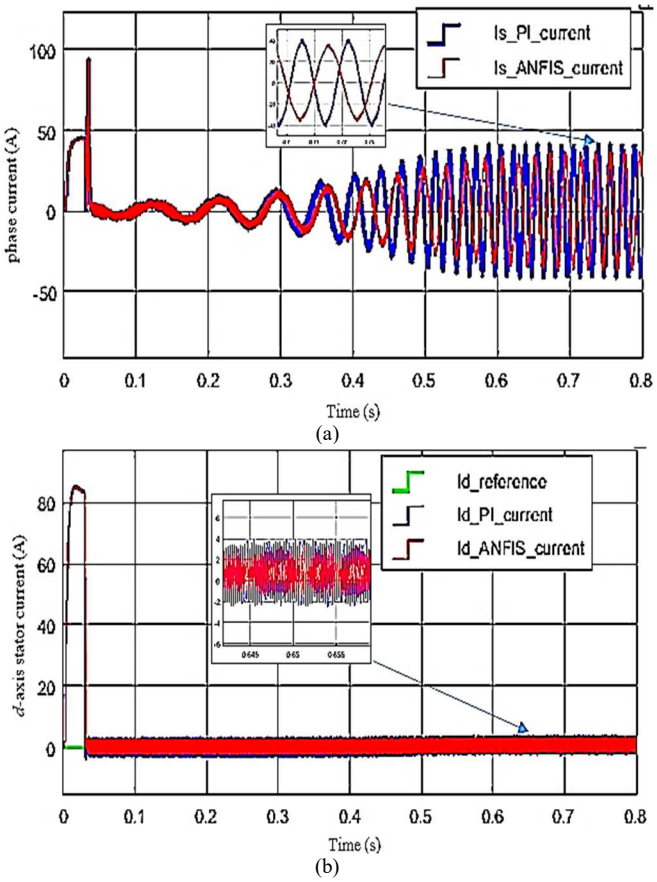

(a)

(b)

Fig. 13 Current performance with a setpoint of 300 rpm 10 Nm.

The phase current THD performance for PI and ANFIS is shown in Fig. 14 (a) and (b), respectively, and the PI had 65.66% while ANFIS had 10.61%, which means there was a difference of 55.05% in the THD value.

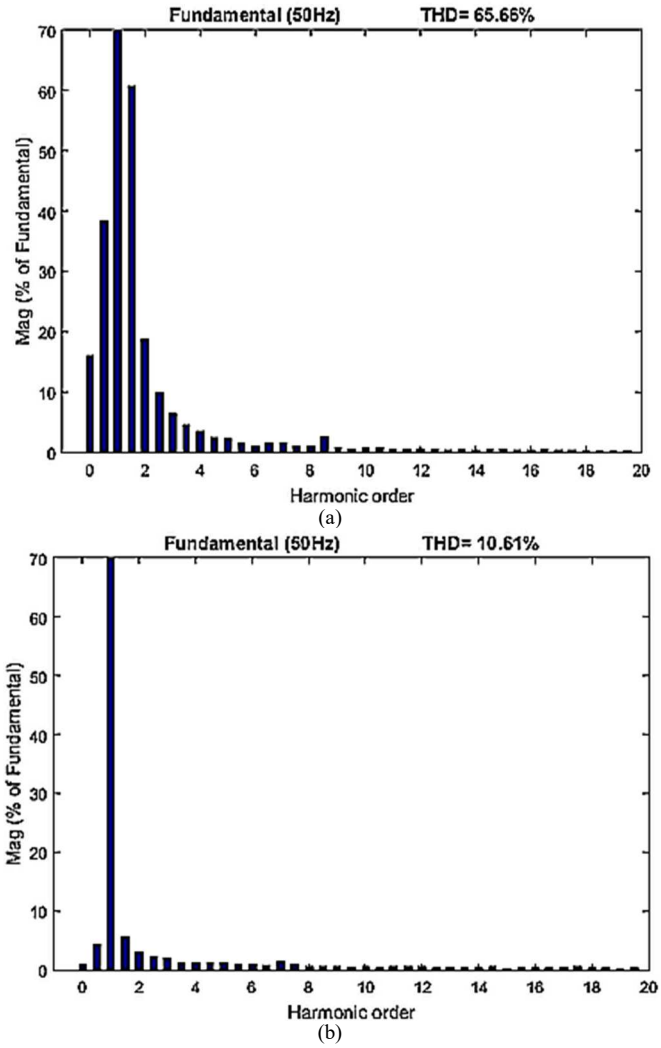

Fig. 14 THD of phase current with 300 rpm setpoint 10 Nm (a) PI *d*-axis SCR (b) ANFIS *d*-axis SCR.

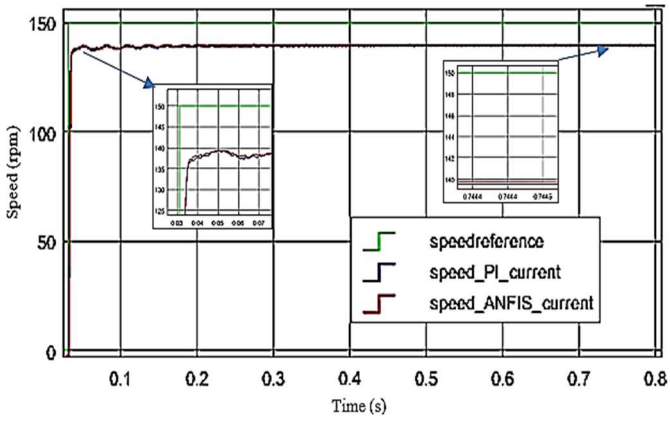

Fig. 15 Speed performance with setpoint of 150 rpm and 30 Nm load.

After several tests were conducted on the set point of 300 rpm, a lower setpoint of 150 rpm was also used at the same constant loads of 30 Nm and 10 Nm. The dynamic performance of the 30 Nm load is shown in Fig. 15 and it was discovered that through the use of PI, IM accelerated to the steady-state speed of 139 rpm with ESS of 7.3% for 0.071 s and a rising time of 0.034 s while ANFIS also showed a steady-state speed value of 139 rpm with ESS of 7.3% at a settling time of 0.072 s and rising time at 0.034 s. This shows both controllers have the same dynamic speed response but are distinguished only by the settling time with a difference of 0.001 s. It was also observed that with the use of a lower speed of 10% rated speed and the same load, ESS has increased compared to the previous test.

Figure 16 shows the performance of IM of phase current at (a) and *d*-axis stator current at (b). Through the use of PI, the phase current response consumed 70.625 A for the peak and 36.64A for the RMS, while ANFIS consumed 64.72 A and 32.91 A, respectively. In this case, phase current consumption both in the peak and RMS values were quite large compared to the two previous cases. Moreover, concerning the error performance of SCR, PI produced IAE of 3.738% with a current ripple from -2 A to 4.5 A while ANFIS produced 3.337% with a current ripple from -1.6 A to 4 A.

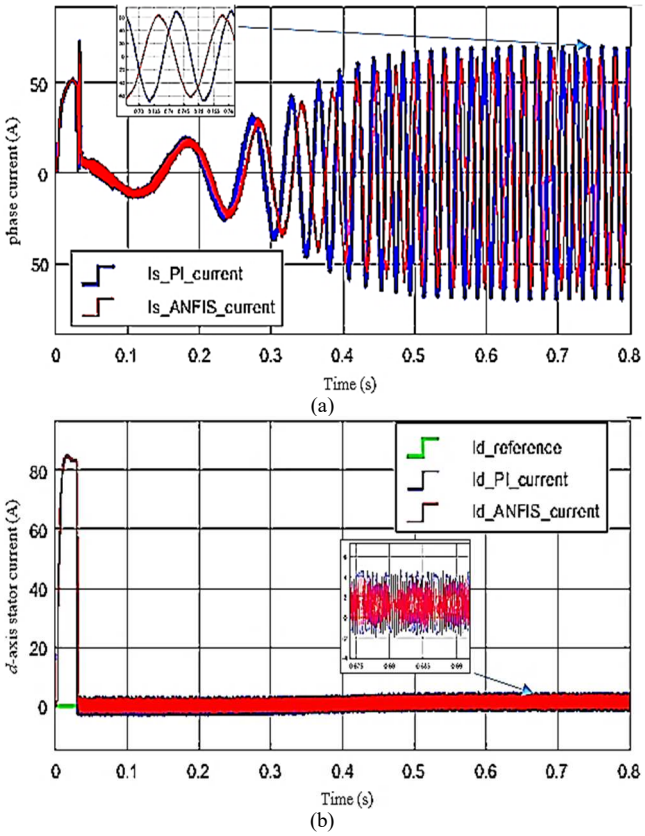

Fig. 16 Current performance with setpoint of 150 rpm 30 Nm.

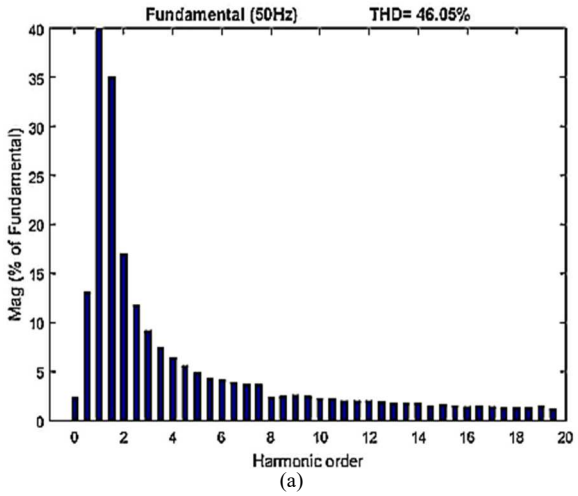

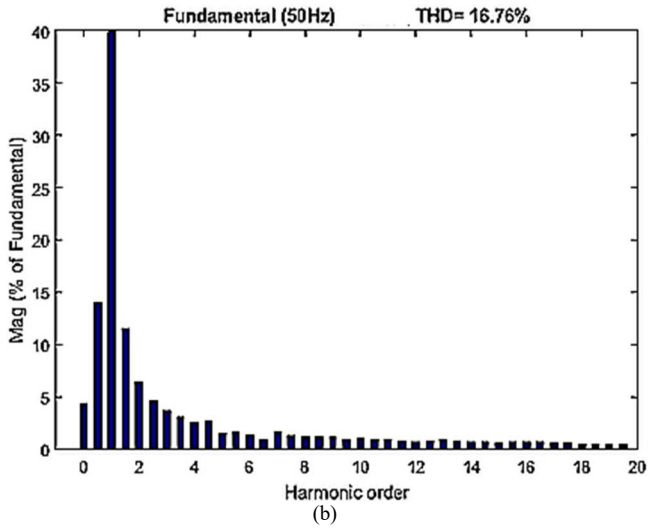

(b)

Fig. 17 THD of phase current with 150 rpm setpoint 30 Nm (a) PI *d*-axis SCR (b) ANFIS *d*-axis SCR.

The phase current THD performance for the 150 rpm setpoint with a load of 30 Nm is shown in Fig. 17 with (a) for PI and (b) for ANFIS. PI was found to have produced a THD of 46.05% while ANFIS produced 16.76% with a fundamental frequency of 50Hz. This indicates a difference in the range of 28.86% between the two controllers.

When the load was changed to 10 Nm at the 150 rpm setpoint, the dynamic speed response performance shown in Fig. 18 found that with PI, the IM accelerated to a steady-state speed of 146 rpm with ESS of 2.66% at 0.048 s with a rising time of 0.034 s while through the use of ANFIS, there was 146 rpm with ESS of 2.66% at a settling time of 0.051 s and rising time at 0.034 s.

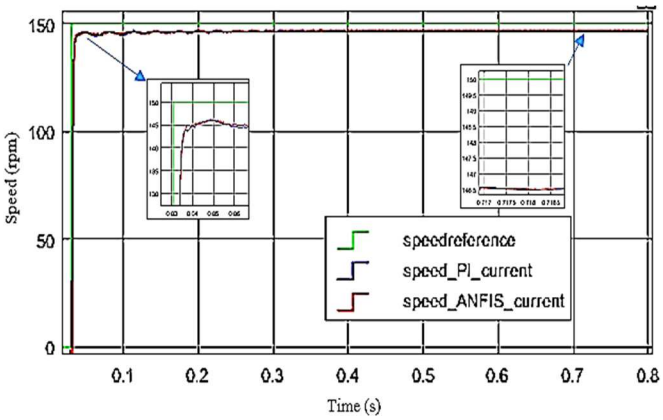

Fig. 18 Speed performance with setpoint of 150 rpm and 10Nm load.

The performance of the phase current performance is shown in Fig. 19 (a) and the *d*-axis stator current in Fig. 19 (b). The PI was observed to have consumed 43.62 A in peak value and 20.49 A in RMS, while ANFIS consumed 37.71 and 17.47 A, respectively, in the phase current. Moreover, regarding the error performance of SCR, the PI produced an IAE of 3.761% with current ripple from -2.2 A to 4 A while ANFIS produced IAE of 3.28% with a current ripple from -1.6 A to 3 A.

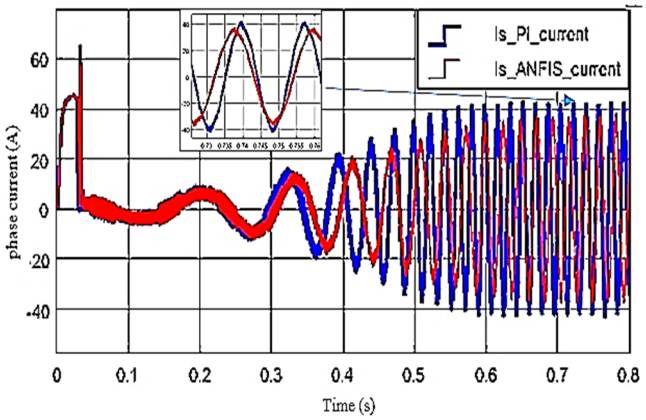

(a)

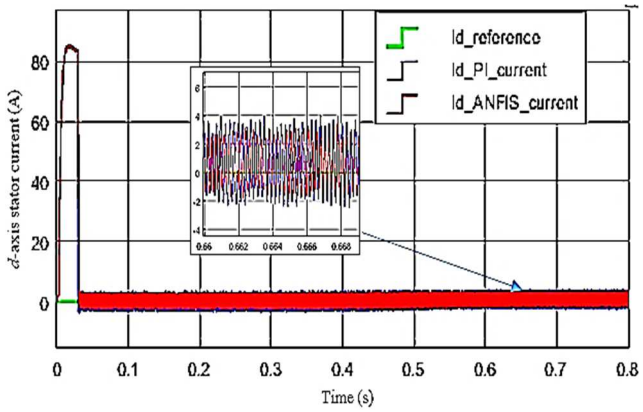

(b)

Fig. 19 Current performance with setpoint of 150 rpm 10 Nm.

Figure 20 shows the phase current THD's performance for *d*-axis SCR with PI in (a) and ANFIS in (b). The PI was discovered to have produced THD of 66.7% while ANFIS had 21.12% with a fundamental frequency of 50Hz. This indicated a difference in the range of 27.53% in this case.

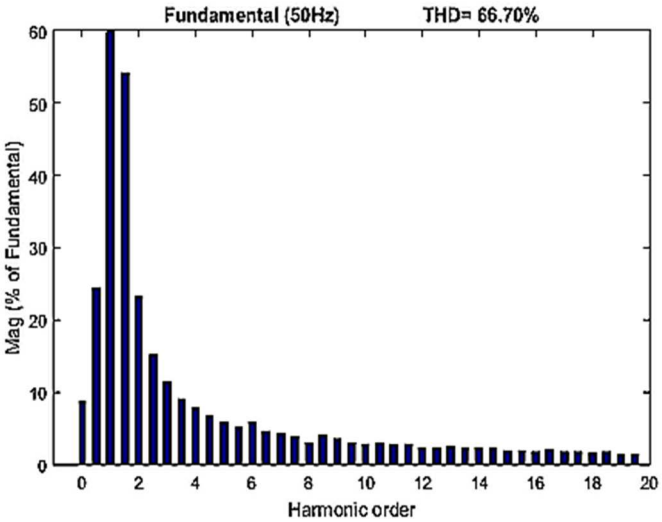

(a)

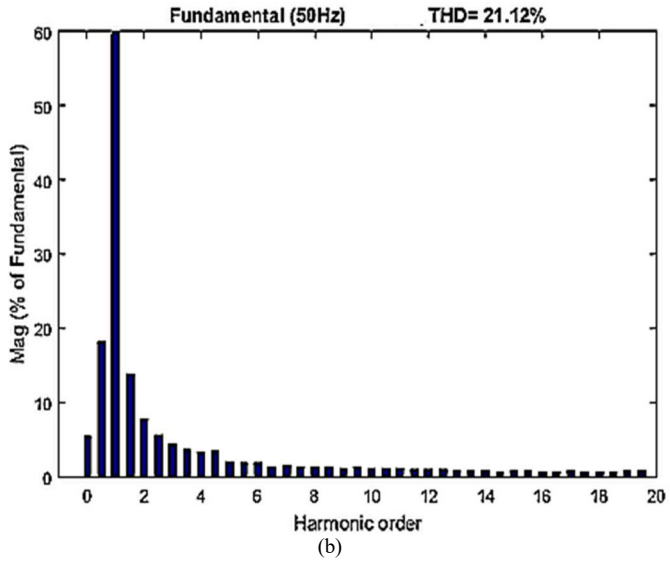

(b)

Fig. 20 THD of phase current with 150 rpm setpoint 10 Nm (a) PI *d*-axis SCR (b) ANFIS *d*-axis SCR.

It was, therefore, possible to evaluate the dynamic speed performance from the values obtained from testing the constant load at 20% and 10% of rated speed setpoints. The steady-state speed value and ESS were observed to have the same values whether using PI or ANFIS in all the setpoints. It was also discovered that the ESS value decreased as the load in the same setpoint was reduced. Moreover, the rising time for setpoint 150 rpm was the same for the two controllers but had different values for 300 rpm, though with a quite small difference of 0.00004 s. The settling time for ANFIS seems faster compared to PI for 300 rpm while the contrary was observed at 150 rpm.

The results of several dynamic speed performance parameters in the constant load test are shown in Table 1 and it was discovered both PI and ANFIS responses have the same speed trend. However, the current consumption by ANFIS is smaller than PI for all setpoints and loads and the same was observed with THD performance from the phase current with ANFIS found to be producing lesser value. Moreover, PI produced bigger IAE than ANFIS with an estimated difference of 0.481% as shown in Table 2.

TABLE I
DYNAMIC SPEED PERFORMANCE EVALUATION

Speed (rpm)	Load (Nm)	TR (s)		Ts (s)		Steady State (rpm)		ESS (%)	
		PI	ANFIS	PI	ANFIS	PI	ANFIS	PI	ANFIS
300	30	0.03486	0.03482	0.106	0.104	289	289	3.6	3.6
	10	0.03472	0.03476	0.122	0.09	296	296	1.3	1.3
150	30	0.034	0.034	0.071	0.072	139	139	7.3	7.3
	10	0.034	0.034	0.048	0.051	146	146	2.6	2.6

TABLE III
CURRENT PERFORMANCE EVALUATION

Speed (rpm)	Load (Nm)	IAE of *d*-axis SCR (%)		Phase Current Peak (A)		Phase Current RMS (A)		THD of Phase Current (%)	
		PI	ANFIS	PI	ANFIS	PI	ANFIS	PI	ANFIS
300	30	3.723	3.331	69.94	63.62	35.89	32.32	59.98	4.44
	10	3.735	3.262	42.41	37.31	20.29	17.51	65.66	10.61
150	30	3.738	3.337	70.62	64.72	36.64	32.91	46.05	16.76
	10	3.761	3.28	43.62	37.71	20.49	17.47	66.7	21.12

B. Dynamic Load

The second test involved constant speed and dynamic load. The IM was operated at a constant speed of 300 rpm with a constant load of 20 Nm and provided with a disturbance of 30 Nm for 0.3 s while the speed and current performance were observed. The IM was first operated at a 300 rpm setpoint with 20 Nm load, and a steady-state speed value of 293 rpm with ESS 2.33% was obtained. At 0.3 s, the load was changed to 30 Nm for 0.3 s, and the speed decreased to 289 rpm with ESS 3.6%. After that, the initial load of 20 Nm was returned, and the same steady-state value and ESS were observed, which means the dynamic speed response trends between PI and ANFIS are the same, as shown in Fig. 21.

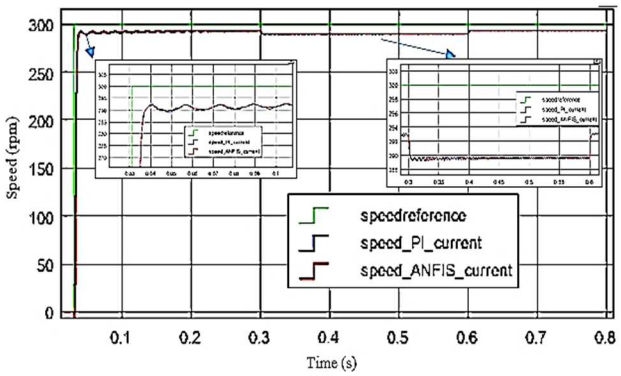

Fig. 21 Speed response of dynamic load with setpoint of 300 rpm.

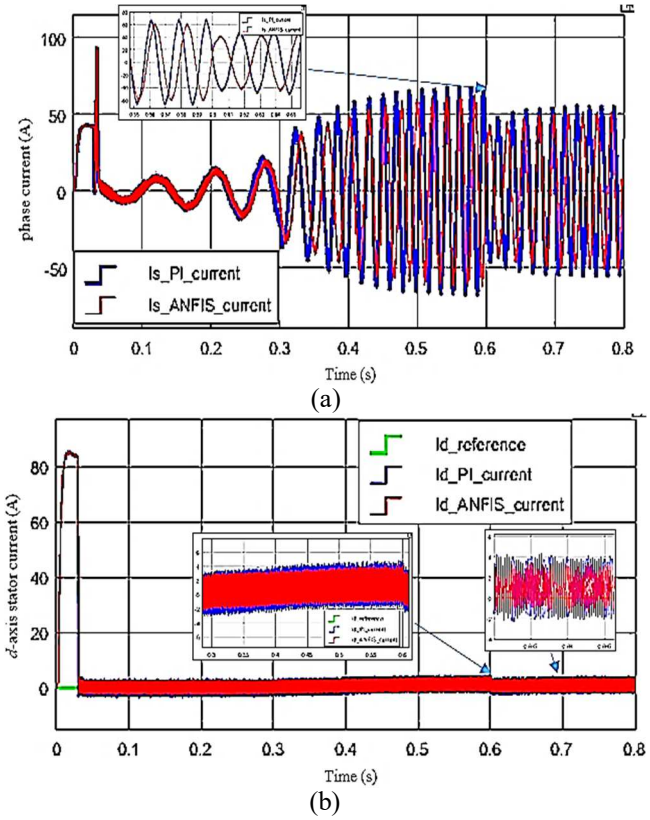

Fig. 22 Current performance with 300 rpm setpoint for dynamic load condition.

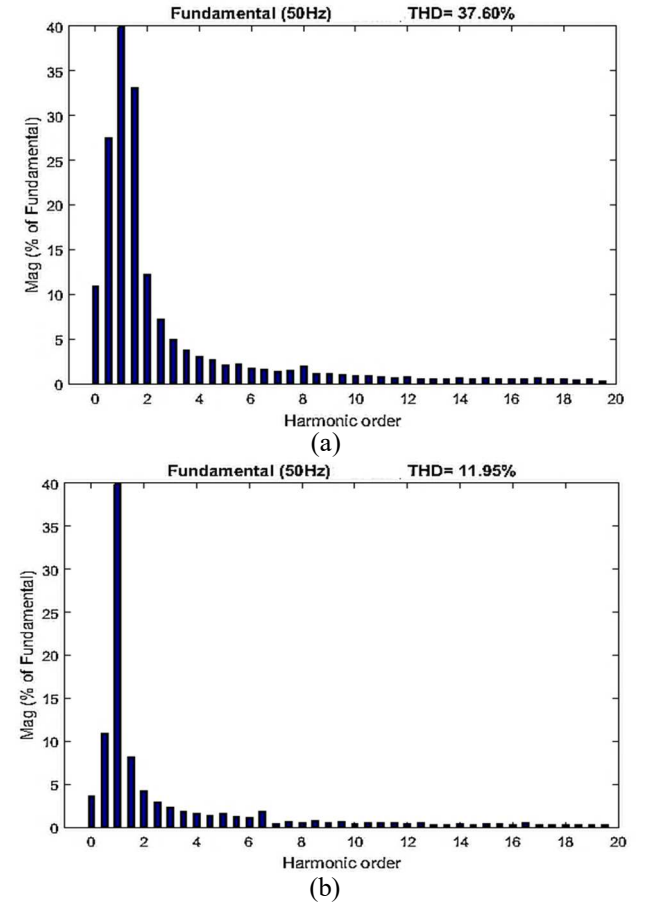

Fig. 23 THD of phase current when testing in dynamic load and measured when the load changes to 30 Nm (a) PI *d*-axis SCR (b) ANFIS *d*-axis SCR.

Regarding the current performance, in peak value, PI was found to have consumed 68.91 A during the load change and 56.23 A when it was reduced to the initial load, while ANFIS consumed 62.49 A and 51.48 A, respectively, in the phase current. This shows a difference of 6.42 A for the phase current consumption during the disturbance period, as shown in Fig. 22.

After the disturbance and achievement of a steady state, the PI consumed 32.42 A while ANFIS consumed 28.95 A in phase current, both in RMS. This indicated a difference of 3.47 A in the RMS current value. Therefore, with the dynamic load test, the current performance in peak and RMS values for ANFIS was smaller. Furthermore, the performance of error in IAE for PI was 3.727% while ANFIS produced 3.304%, and this showed a difference of 0.423% in this case. In the disturbance period, phase current THD was observed, and the PI was found to have 37.6%, while ANFIS had 11.95% as shown in Fig. 23 (a) and (b) respectively. This, therefore, showed a difference in the range of 25.65%.

IV. Conclusion

ANFIS controllers for *d*-axis SCR was designed and implemented on 10 HP IM drives based on IFOC through MATLAB/Simulink. The performance of dynamic speed, current consumption in peak and RMS value, SCR error performance, and the phase current THD under low-speed operating conditions of 10-20% of rated speed were analyzed while ANFIS SCR was compared with PI SCR. The PI and ANFIS were discovered to have produced the same speed response trend from both constant and dynamic load tests. However, there was a reduction of 2.78 A - 6.32 A in phase currents consumption, both in peak and RMS value. Furthermore, a decrease in the range of 25.65% - 55.54% was also observed for THD. Therefore, the application of ANFIS-based SCR on IFOC was found to have the ability to optimize current ability and ensure high performance for IM drives in low-speed operations.

Acknowledgment

The Indonesia Government grant fully supports this research. The authors fully acknowledged the Ministry of Research, Technology and Higher Education for the approved fund, making this important research viable and effective.

References

[1] Ferdiansyah, I.; Rusli,M.R.; Praharsena,B.;Toar,H.; Ridwan; and Purwanto,E.(2018). Speed Control of Three Phase Induction Motor Using Indirect Field Oriented Control Based on Real-Time Control System. Proceedings of2018 10th International Conference on Information Technology and Electrical Engineering (ICITEE). Kuta,438-442.

[2] Praharsena,B.; Purwanto,E.; Jaya,A.; Rusli, M.R.; Toar, H.; and Ridwan(2018). Stator Flux Estimator Using Feed-Forward Neural Network for Evaluating Hysteresis Loss Curve in Three Phase Induction Motor.EMITTER International Journal of Engineering Technology,6(1), 168-184.

[3] Praharsena,B.; and et al.(2018). Evaluation of Hysteresis Loss Curve on 3 Phase Induction Motor by Using Cascade Feed Forward Neural Network.Proceedings of2018 International Electronics Symposium on Engineering Technology and Applications (IES-ETA). Bali, 117-122.

[4] Bennassar, A.; Abbou, A.; Akherraz, M.;and Barara, M.(2016). "Fuzzy Logic Based Adaptation Mechanism for Adaptive Luenberger Observer Sensorless Direct Torque Control Of Induction Motor."

Journal of Engineering Science and Technology (JESTEC),11(1), 46-59.
[5] Hannan, M.A.;Ali, J.A.;Mohamed, A.; and Hussain, A. (2018).Optimization techniques to enhance the performance of induction motor drives: A review.Renewable and Sustainable Energy Reviews,81(2), 1611-1626.
[6] Zhang, B.; Liang, B.; Xu, G.; Wang, W.; and Feng, G. (2011). Research on variable frequency low-speed high-torque squirrel cage induction machine for elevator. Proceedings of 2011 International Conference on Electrical Machines and Systems.Beijing, 1-5.
[7] Munoz-Garcia, A.; Lipo, T.A.; and Novotny, D.W. (1998). A new induction motor V/f control method capable of high-performance regulation at low speeds.IEEE Transactions on Industry Applications,34(4), 813-821.
[8] Lee, D.-C.; Sul, S.-K.; and Park, M.-H. (1994). High performance current regulator for a field-oriented controlled induction motor drive.IEEE Transactions on Industry Application,30(5), 1247-1257.
[9] Briz, F.; Diez, A.; Degner, M.W.; and Lorenz, R.D. (2001). Current and flux regulation in field-weakening operation [of induction motors]. IEEE Transactions on Industry Applications,37(1), 42-50.
[10] Quang, N.P.;and Dittrich, J.-A. (2015). Vector Control of Three-Phase AC Machines.Heidelberg:Springer-Verlag Berlin.
[11] Rashid, M. (2017). Power Electronics Handbook (Fourth Edition). Saint Louis: Butterworth-Heinemann.
[12] Krishnan, R. (2001). Electric Motor Drives: Modeling, Analysis, and Control.Prentice Hall.
[13] Hannan, M.A.; Ali, J.A.; Mohamed A.; Amirulddin, U.A.U.; Tan,N.M.L.; and Uddin, M.N.(2018). Quantum-Behaved Lightning Search Algorithm to Improve Indirect Field-Oriented Fuzzy-PI Control for IM Drive. IEEE Transactions on Industry Applications,54(4), 3793-3805.
[14] Ali, J.A.; Hannan, M.A.; and Mohamed, A. (2016). Improved Indirect Field-Oriented Control of Induction Motor Drive Based PSO Algorithm. Jurnal Teknologi,78(6-2), 27-32.
[15] Aditya, A.W.; Happyanto, D.C.; and Sumantri, B. (2017). Application of Sliding Mode Control in Indirect Field Oriented Control (IFOC) for Model Based Controller. EMITTER International Journal of Engineering Technology,5(2), 255-269.
[16] Aditya, A.W.; Rusli, M.R.; Praharsena, B.; Purwanto, E.; Happyanto, D.C.; and Sumantri, B. (2018). The Performance of FOSMC and Boundary - SMC in Speed Controller and Current Regulator for IFOC-Based Induction Motor Drive.Proceedings of 2018 International Seminar on Application for Technology of Information and Communication.Semarang, 139-144.
[17] Talib, M.H.N.; Ibrahim, Z.; Rasin, Z.; Lazi, J.M.;and Azri, M. (2017). Investigation of Different Rules Size FLSC Performance Applied to Induction Motor Drive. Journal of Telecommunication, Electronic and Computer Engineering,9(2-8),165-169.
[18] Salleh, Z.; Sulaiman, M.; and Omar, R. (2016). Tuning Fuzzy Membership Functions to Improve Performance of Vector Control Induction Motor Drives.Journal of Telecommunication, Electronic and Computer Engineering,8(2), 1-4.
[19] Azcue-Puma, J.L.; Sguarezi Filho,A.J.; and Ruppert, E.(2013). Direct-FOC with Fuzzy Current Control for asynchronous machine. Proceedings of 2013 IEEE International Conference on Industrial Technology (ICIT). Cape Town, 307-312.
[20] El-Sousy, F.F.M.; and Nashed, M.N.F. (2003). Robust Fuzzy Logic Current and Speed Controllers for Field-Oriented Induction Motor Drive. Journal of Power Electronics,3(2), 115-123.
[21] Boussada, Z.; Hamed, M.B.; and Sbita, L.(2014). Adaptive neuro-fuzzy inference system into induction motor: Estimation.Proceedings of 2014 International Conference on Electrical Sciences and Technologies in Maghreb (CISTEM). Tunis, 1-5.
[22] Kılıç, E.; Yılmaz, Ş.; Özçalık, H.R.; and Şit, S. (2000). A comparative analysis of FLC and ANFIS controller for vector controlled induction motor drive.Proceedings of 2015 Intl Aegean Conference on Electrical Machines & Power Electronics (ACEMP), 2015 Intl Conference on Optimization of Electrical & Electronic Equipment (OPTIM) & 2015 Intl Symposium on Advanced Electromechanical Motion Systems (Electromotion).Side, 102-106.
[23] Mechernene, A.; Zerikat, M.; and Chekroun, S. (2010). Indirect field oriented adaptive control of induction motor based on neuro-fuzzy controller. Proceedings of 18th Mediterranean Conference on Control and Automation.Marrakech, 1109-1114.
[24] Mishra, R.N.; and Mohanty, K.B. (2016). Real time implementation of an ANFIS-based induction motor drive via feedback linearization. Engineering Science and Technology, an International Journal,19(4), 1714-1730.
[25] Hussain,S.; and Bazaz, M.A.(2014). ANFIS implementation on a three phase vector controlled induction motor with efficiency optimisation.Proceedings of 2014 International Conference on Circuits, Systems, Communication and Information Technology Applications (CSCITA). Mumbai, 391-396.
[26] Nour, M.; and Too, S.Y. (2006). Adaptive Fuzzy Logic Speed Controller With Torque Adapted Gains Function for PMSM Drive.Journal of Engineering Science and Technology (JESTEC),1(1), 59-75.
[27] Gupta, R.A.; Kumar, R.; and Surjuse, R.S. (2009). ANFIS Based Intelligent Control of Vector Controlled Induction Motor Drive.Proceedings of 2009 Second International Conference on Emerging Trends in Engineering & Technology.Nagpur, 674-680.
[28] Duarte-Mermoud, M.A.; and Prieto, R.A. (2004). Performance index for quality response of dynamical systems. ISA Transactions,43, 133-151.